Mechatronics 22 (2012) 890–903

Contents lists available at SciVerse ScienceDirect

Mechatronics

journal homepage: www.elsevier.com/locate/mechatronics

Optimal design of MR damper via finite element analyses of fluid dynamic and magnetic field

Zekeriya Parlak *, Tahsin Engin, İsmail Çallı

Department of Mechanical Engineering, Sakarya University, 54187 Sakarya, Turkey

ARTICLE INFO

Article history:
Received 21 February 2011
Accepted 19 May 2012
Available online 19 June 2012

Keywords:
Magnetorheological fluid
MR damper
MR fluid
Finite element
Magnetic field
Computational fluid dynamics
CFD

ABSTRACT

In the last decade many researchers have been carried out on semi-active control systems, a large number of academic publications have been presented. Semi-active control systems which are used the magnetic field controlled fluid have been shown significant improvements by the researchers. In the study, a design optimization method that has been carried out for the objectives of target damper force and maximum magnetic flux density of an MR damper has been presented. Finite element methods, electromagnetic analysis of magnetic field and CFD analysis of MR flow, have been used to obtain optimal value of design parameters. The new approach that is use of magnetic field and MR flow together and simultaneously has specified optimal design values. Two optimal design of MR damper obtained have been verified with experimental study by manufacturing and testing of the dampers.

1. Introduction

Semi-active controllable devices with magnetorheological (MR) fluid have drawn significant attention especially in transportation vehicles, building suspensions and biomedical applications in the last two decades owing to their unique advantages. MR fluids are suspensions of magnetically polarizable particles with a few microns in size dispersed in a carrying liquid such as mineral or silicon oil.

Recently, some studies in literature have been focused on the modelling and control strategy of MR devices. Design methods that can decrease the cost and the manufacturing period and improve the performance have been more important. Many factors need to consider in developing of MR damper to obtain optimal designs, which makes the problem very challenging when using conventional optimization methods.

Wereley and Pang [1] developed a quasi-static model based on the Bingham plastic model. They characterized the damper performance using the control ratio that depends on nondimensional numbers, which are the Bingham number and ratio of plug thickness. Felt et al. [2] and Dimock et al. [3] observed that the Bingham plastic model is inadequate to describe the shear-thinning flow that is seen in MR fluid. Hesselbach and Abel-Keilhack [4] implemented flow simulations of the MR fluid using three flow models consisting of the Bingham, the Herschel–Bulkley and the Bi-Bingham. Wang [5] carried out analytical flow analysis of the MR fluid devices using the Herschel–Bulkley model. Wang and Gordaninejad [6] improved a model to calculate pressure through pipes and parallel plates in which the MR fluid flows. Yasrebi et al. [7] presented an electromagnetic and flow finite element analysis of a MR damper using ANSYS codes. They modelled only the annular gap that is between cylinder and piston head, where is subjected the magnetic field, in the flow analysis. Widjaja et al. [8] developed a mathematical model based on the Herschel–Bulkley model to describe flow characteristic that cannot be obtained as experimentally. They showed thanks to the model that the gap size of less than 1 mm causes a significant increase of the damper force. Ericksen and Gordaninejad [9] presented a theoretical fluid mechanics-based model to predict the controllable damping force in terms of the physical parameters of the device, the MR fluid properties, the electromagnetic circuit parameters, and the input motion for semi-active suspension systems of off-road motorcycle. Li and Du [10] investigated yield stress of a MR brake system experimentally based on Bingham Plastic model. Ellam et al. [11] investigated two-dimensional steady isothermal flows of a Bingham plastic fluid between two plates, one moving and the other stationary. A commercial CFD package was used to verify for similar flows in more complex situations including heat transfer, electrical conductance, thermal and shear rate effects on fluid properties, and unsteady motion. Susan-Resiga [12] presented blending rheological model of a MR fluid that is related to Newtonian and non-Newtonian behaviours at very low shear stress and large shear stress, respectively. The Herschel–Bulkley model was used for value

* Corresponding author. Tel.: +90 2642955495; fax: +90 2643460080.
E-mail address: zparlak@sakarya.edu.tr (Z. Parlak).

0957-4158/$ - see front matter © 2012 Elsevier Ltd. All rights reserved.
http://dx.doi.org/10.1016/j.mechatronics.2012.05.007

of large shear stress where the suspension displays a shear-thinning behaviour. The model parameters allow the identification of a yield point, which MR fluid passes to non-Newtonian type from Newtonian type, on the flow curve (shear stress vs. shear rate). They explained that their model could be used in regular CFD codes to compute the MR fluid flow in practical applications.

Hitchcock [13] found performing a 3D FEM analysis, and reported that the magnetic field direction should be perpendicular to the MR fluid flow direction. Zhang et al. [14] proposed a design method for the MR dampers based on FEM. They showed by experimental verification, the damper force was effectively scaled by the magnetic design. Nguyen et al. [15] applied the optimal design model for single-coil, two-coil, three-coil and radial–annular types of the MR valves constrained in a specified volume. They found that two-coil MR valve provided the best value of valve ratio while the annular–radial type provides the best pressure drop at the optimal design parameters. Nguyen et al. [16] proposed a similar model for the MR valve but considering the control energy as well as the time response. Nguyen and Choi [17] extended the previous research works [15,16] to vehicle MR dampers considering an advanced objective function which includes the damping force, the dynamic range, and the inductive time constant altogether. Also, Nguyen and Choi [18] presented an optimal design of a MR shock absorber based on FEM. The MR shock absorber was constrained in a specific volume and the optimization problem identified the geometric dimensions of the shock absorber that minimize a multi-objective function. They determined the optimal values for the coil width, flange thickness, piston radius and gap width. Yang et al. [19] introduced an MR smart structure design method. In their optimization procedure, the objective function was selected as the damping force, and the volume fraction, target time constant, magnetic field intensity, wire winding turns, lost power were chosen as constraints. They determined the optimal values of for damping force, the magnetic field intensity, time constant and lost power for various wire winding turns at constant cylinder diameter, length and gap. Karakoc et al. [20] worked on design considerations for building an automotive MR brake. They performed a FEM analysis to analyses the resulting the magnetic circuit and heat distribution within the MR brake and a design optimization procedure to obtain optimal design parameters that can generate the maximum braking torque in the brake. Grunwald and Olabi [21] presented the parametrical analysis, which is used optimization purpose, with magnetic simulations of a MR valve and a MR orifice. Based on the analyses they designed, fabricated and tested the devices.

In our brief study [22] was dealt with the geometrical optimization of an MR shock damper using the Taguchi method. Four parameters were specified for the optimization and dynamic range to be desired at maximum value was target value. It was performed the analysis using analytical equations instead of experimental study.

The present study deals with a new optimization strategy of an MR damper based on the Finite Element method (FEM), electromagnetic analysis of magnetic field and CFD analysis of fluid flow are used to obtain optimal value of design parameters. Unlike the existing optimization methods, this approach can specify optimal value of parameters by using a magnetic field and MR flow together and simultaneously. Thus, physics of magnetic field and fluid flow of MR damper are considered in the optimization method. Two objectives, a target damper force and maximum magnetic flux density, are determined to get the optimal values in FEM analyses. The finite element analyses are realized with ANSYS v12.1, which is also used for optimization tool, as three-dimensional in the study. The main contribution of the study is to propose a new approach to optimize of an MR device that use of FEM analyses of the magnetic field and fluid flow together and simultaneously. When applied a current excitation on MR damper, distribution, direction and magnitude of the magnetic field are specified by the finite element analysis. Values of the magnetic field intensity convert to values of the yield stress to use in the flow analysis. CFD analysis in the study that is implemented with deformed (moving) mesh approach by taking into consideration movement of the piston. While moving piston, numerical and visual results of fluid flow in the MR damper are obtained by the CFD analysis, then damper force can be calculated. In addition, in the CFD analysis, non-Newtonian flow in the annular gap of piston head of the MR damper due to the magnetic field is modelled using the Bingham CFD model by taken into consideration piston position due to moving firstly presented in the study. The optimal damper configurations obtained after the optimization study are manufactured and tested.

2. MR fluids

When a magnetic field is applied to the fluid, particles in the fluid form chains, and the suspension becomes like a semi-solid material in a few millisecond. Under the magnetic field, an MR fluid behaves as a non-Newtonian fluid with controllable viscosity. However, if the magnetic field is removed, the suspension turns to a Newtonian fluid and the transition between these two phases is highly reversible, which provides a unique feature of magnetic-field controllability of the flow of MR fluids. The chains form causes about 50 kPa of yield stress depending on type of MR fluids in a few millisecond, the case creates a resistance against the fluid flow.

If a force is applied on the chains form, the shape of the form changes in terms of magnitudes of the force and magnetic field. The pressure reaction on MR fluid is called "MR effect". In Fig. 1 as can be seen that the particles are scattered randomly in the liquid carrier, when magnetic field applied, the particle array in the direction of the magnetic flux lines to resist the flow (Fig. 1b), and the chains form is changed in term of force applied to the particles (Fig. 1c).

Properties of hydrocarbon-based MR fluid product (MRF-132DG) used in the study can be seen Table 1 [23].

2.1. Flow models of MR fluid

MR fluid can be modelled by nonlinear models such as the Bingham plastic.

The Bingham plastic model;

$$\begin{aligned} \tau &= \tau_y(B)sgn(\dot{\gamma}) + \mu_p\dot{\gamma} \quad |\tau| > \tau_y \\ \dot{\gamma} &= 0 \quad |\tau| < \tau_y \end{aligned} \tag{1}$$

where τ is shear stress, $\dot{\gamma}$ (du/dr) is shear rate, τ_y (B) is yield stress changing with magnetic flux intensity, μ_p is plastic viscosity independent on magnetic field.

Behaviours of the MR fluid when active in other words under the magnetic field in the gap, the fluid acts like a rigid body below dynamic yield stress considering the Bingham plastic model. This plug region is called the pre-yield. In the pre-yield region, the local shear stresses have not yet exceeded the dynamic yield stress. When the local shear stresses exceed the dynamic yield stress, these regions are called the post-yield region and then the fluid acts like a viscous fluid. The pre- and post-yield regions are shown in Fig. 2 with the velocity profile. As can be seen in Fig. 2, the velocity profile is divided into three regions: Region I and III denote the post-yield regions and Region II denotes the pre-yield region [24].

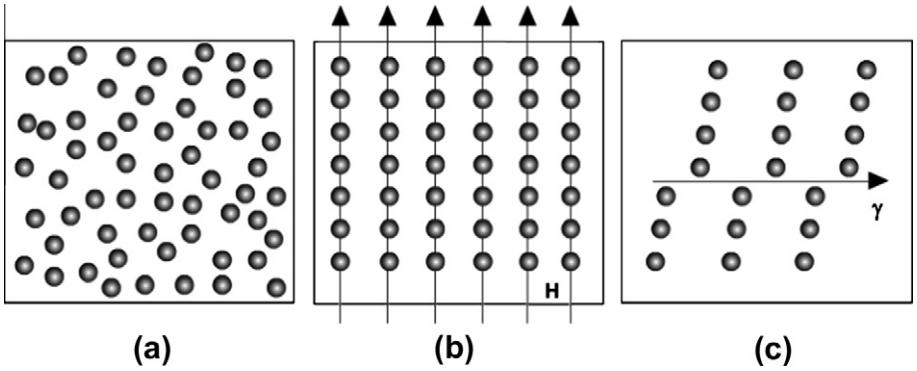

Fig. 1. MR effect.

Table 1
Properties of MRF-132DG.

Property	Value/limits
Base fluid	Hydrocarbon
Density	3090 (kg/m^3)
Coefficient of thermal expansion	
0–50 (°C)	5.5e−4
50–100 (°C)	6.6e−4
100–150 (°C)	6.7e−4
Specific heat at 25 (°C)	800 (J/kg K)
Thermal conductivity 25 (°C)	0.25–1.06 (W/m K)
Viscosity	0.09 (±0.02) Pa s

3. MR damper

MR dampers have attracted the interest of researchers because of their variable damping feature, mechanical simplicity, low power consumption, fast response and complying with electronic control.

Fig. 3 shows a schematic for the prototyped the MR damper consisting of two chambers in the cylinder separated by a sliding piston. A section of the piston head is filled with MR fluid, and the other section is an accumulator, which is for compensating the volume changes induced by the movement of the piston rod to the up and down, is filled with the pressurized nitrogen gas. While moving the MR damper's piston rod, the fluid flows the other side of piston head through the annular gap. Inside the piston head, a coil is located and coil wire used for winding is heat-resistant and electrically insulated. When electrical current is applied to the coil, a magnetic field occurs around the piston head.

The controllability of the MR damper is provided by varying the excitation current. When the MR fluid is activated a plug region occurs in the gap, the remaining unbound fluid does great shear force that causes a pressure drop though the gap that is energy loss due to the magnetic field and viscosity.

Typically, the MR devices have generally one annular gap through which fluid is forced, but this is not a strict constraint. In numerous papers single rectangular and annular ducts and concentric multiple annular gaps were employed in the devices. The fail-safe design feature is accomplished by selecting appropriate

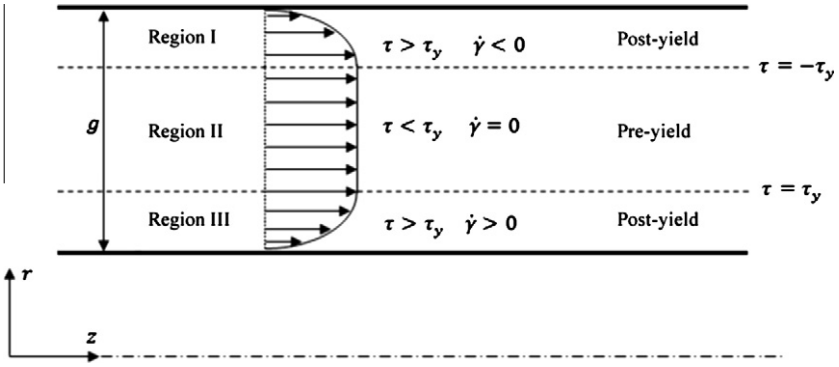

Fig. 2. Velocity profiles across the annular duct.

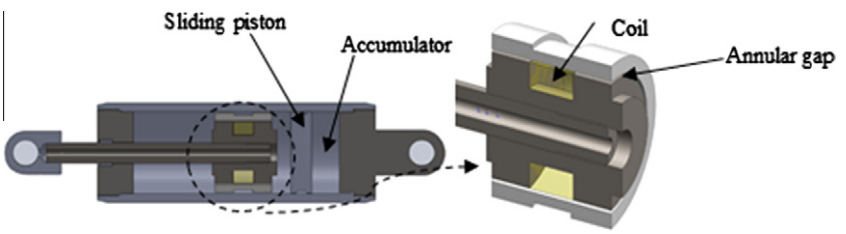

Fig. 3. Schematic for the prototyped MR shock damper.

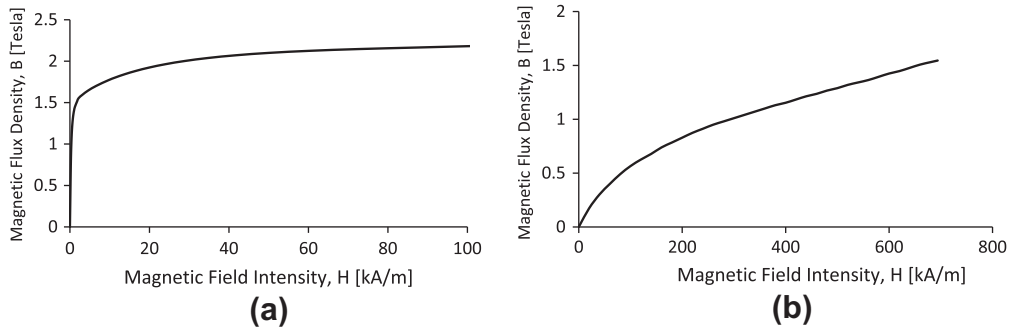

Fig. 4. (a) B–H curve of C1010 steel (b) B–H curve of MRF-132DG.

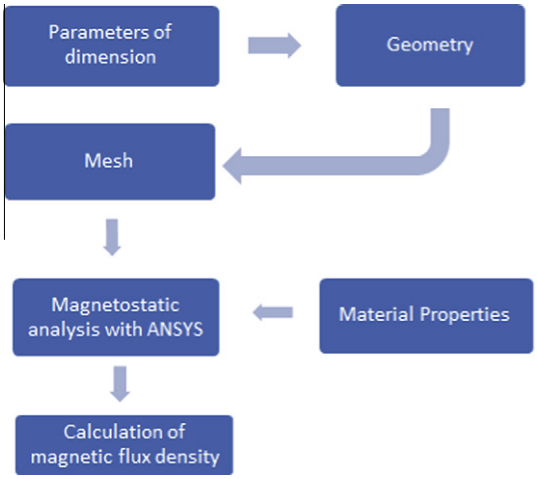

Fig. 5. Steps of calculation of magnetic flux density.

channel flow geometry to obtain the minimum required viscous (passive) damping force at zero magnetic field [13]. Rosenfeld and Wereley [25] assumed that the off-state damping requirement had been fixed (e.g., by safety requirements for minimum damping), and that the damper should achieve the greatest possible on-state damping.

In the study, a damper with one-coil, annular gap and volume-constrained was used by also considering manufacturing simplification. However, the gap width, active flange length, piston head housing thickness, radius of piston core, coil width, gap length, and coil wire diameter were specified as variables to obtain optimal damper geometry.

3.1. Controllable force and the dynamic range

The total force generated by an MR damper consists of three components: viscous force (uncontrollable force) due to the viscous effects F_μ, friction force F_f and field dependent force (controllable force) F_τ due to magnetic field [26].

$$F = F_\mu + F_\tau + F_f \tag{2}$$

where

$$F_\mu = u_p(A_p - A_r)\frac{6\mu_p L A_p}{\pi R_1 g^3} \tag{3}$$

$$F_\tau = 2c\frac{t}{g}A_p\tau_y sgn(u_p) \tag{4}$$

where u_p is piston velocity, A_p is cross-section area of the piston head, A_r is cross-section area of piston road, μ_p is plastic viscosity, L is the annular gap length of the piston head, R_1 is the average radius of the annular gap, g is annular gap width, t is active (pole) length exposed to the magnetic field, c is the coefficient that depends on the flow velocity profile and τ_y is yield stress that function of magnetic field intensity. Dynamic range, D, is defined as the ratio of the total damper force to the uncontrollable force:

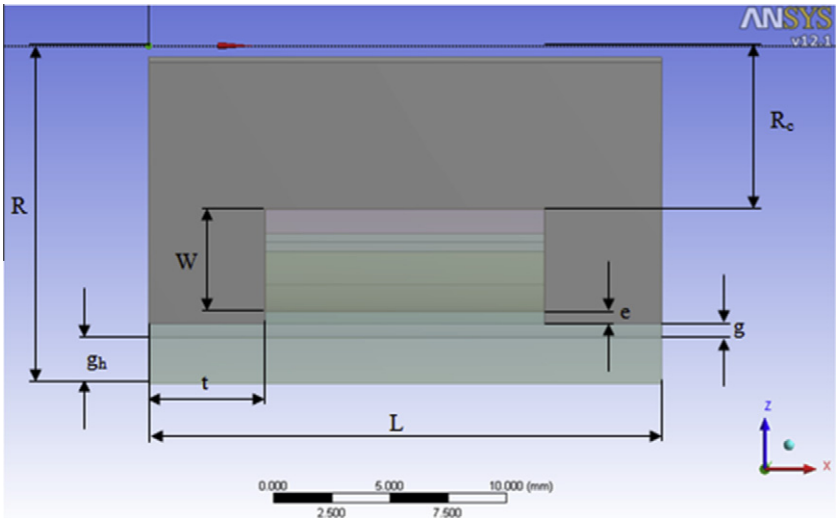

Fig. 6. Geometrical sizes of the piston head.

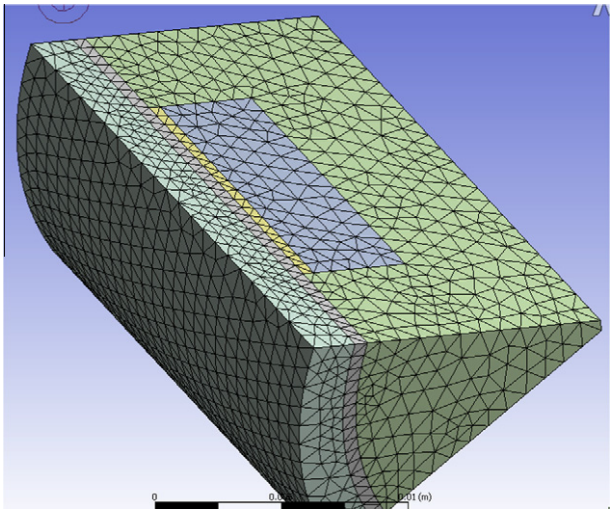

Fig. 7. Meshes of the piston head.

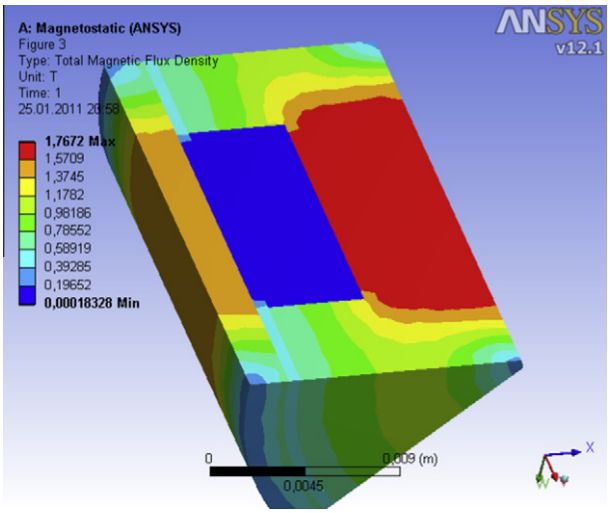

Fig. 8a. Magnetic flux density.

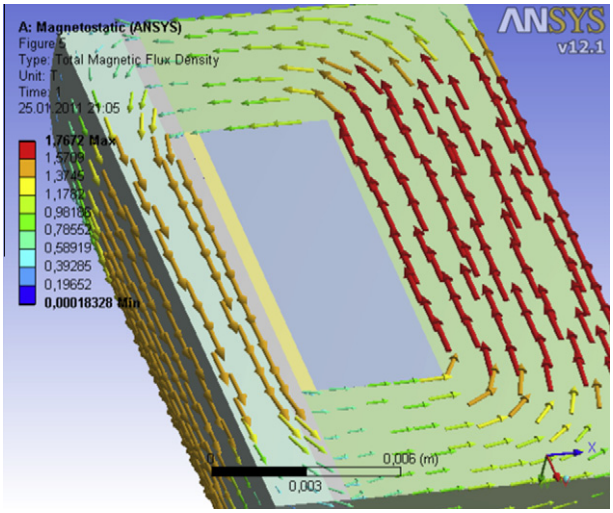

Fig. 8b. Directions of magnetic flux.

Table 2
Value of magnetic flux density and yield stress.

g (mm)	t (mm)	d_k (mm)	I (A)	W (mm)	N_c	B (T)	τ_y (Pa)
0.6	5	0.45	1	4.9	220	0.563	32.02

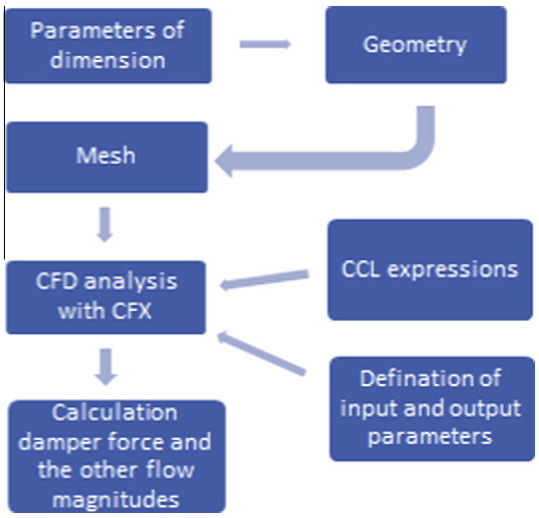

Fig. 9. The steps for fluid flow.

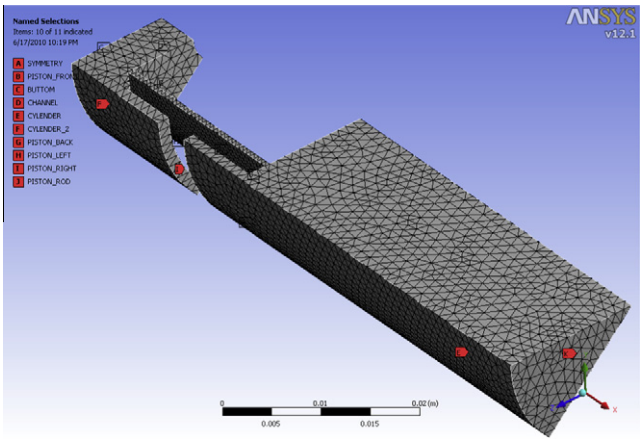

Fig. 10. Mesh and boundaries of computational domain.

$$D = 1 + \frac{F_\tau}{F_\mu + F_f} \tag{5}$$

The dynamic range is introduced to evaluate the overall performance of an MR damper: D is desired as large as possible to maximize the effectiveness of an MR damper. Parameters such as the piston radius, the yield stress, pole length and the gap width will play an important role in searching for the right design.

The magnetic circuit design provided changes in the yield stress of the MR fluid is one of the most important stage in the design considerations of an MR damper. In this study, MRF-132DG from Lord Corporation was used. By applying the least-squares curve fitting method to the fluid property specifications [27] the yield stress is determined to be

$$\tau_y = 52.962B^4 - 176.51B^3 + 158.79B^2 + 13.708B + 0.1442 \tag{6}$$

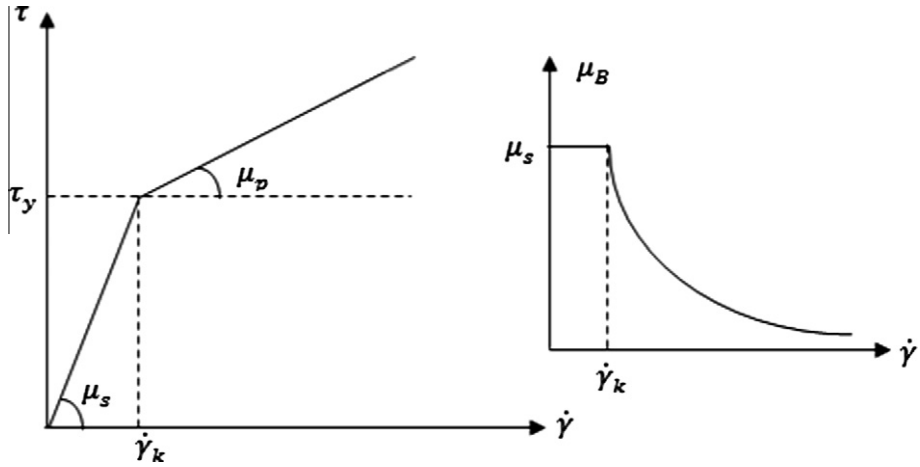

Fig. 11. Bingham CFD model.

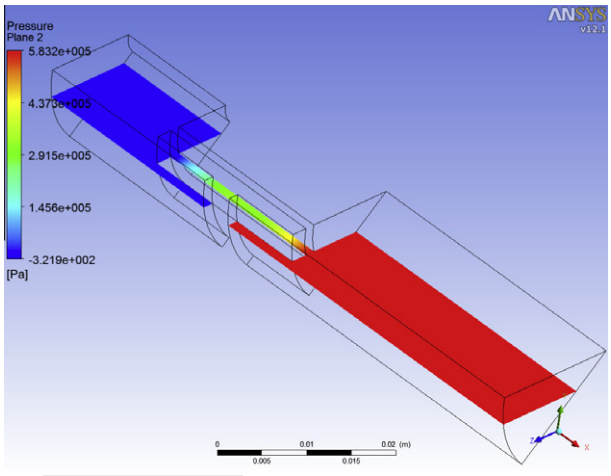

Fig. 12. Variation of pressure on a plane at 0.36 s.

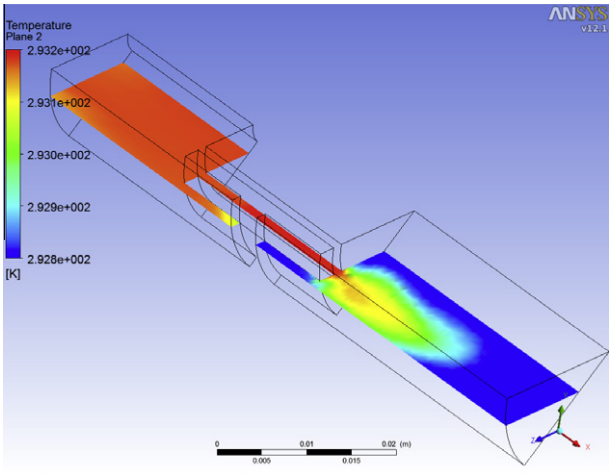

Fig. 14. Variation of temperature on a plane at 1.12 s.

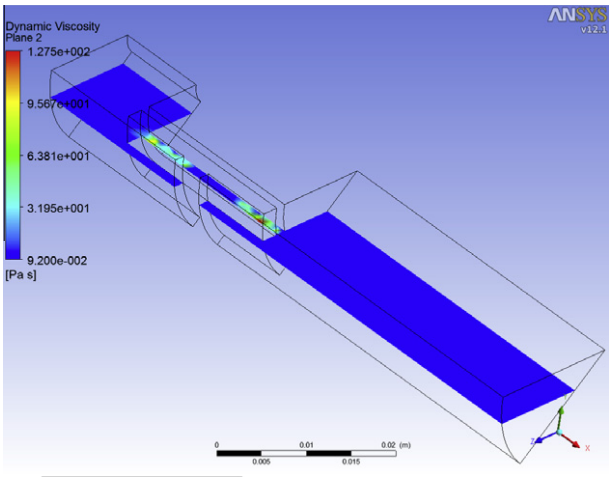

Fig. 13. Dynamic viscosity on a plane at 0.26 s.

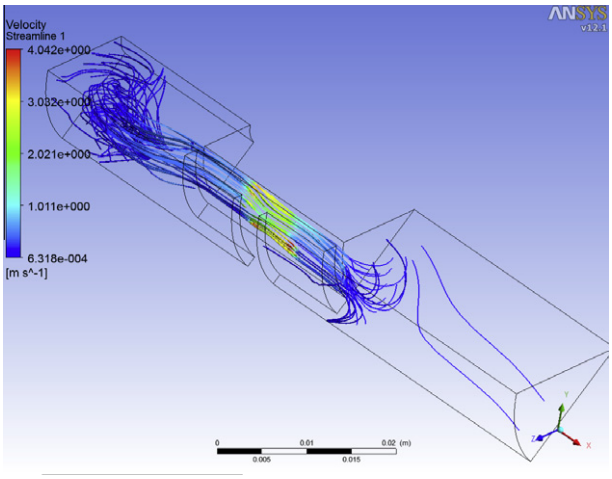

Fig. 15. Streamlines at 0.45 s.

In Eq. (6), the unit of the yield stress τ_y is kPa while that of the magnetic flux density is Tesla (T). The magnetic flux density of the MR fluid can be approximated by Nguyen and Choi [28]

$$B = \frac{\mu_0 N_c I}{2\frac{g}{\mu_{r,m}}} \tag{7}$$

where μ_0 is the magnetic permeability of free space, I is current, $\mu_{r,m}$ is the relative permeability of MR fluid. N_c is number of coil turns.

Low carbon steels that have a high magnetic permeability and saturation are desired to design the magnetic circuit of the MR sys-

tems. In the study, low carbon steel C1010 steel was used in the cylinder, coil housing and piston head materials. B–H (Magnetic flux density–Magnetic field intensity) curves of the C1010 [29] and the MRF-132DG [23] can be seen in Fig. 4.

4. Calculation of magnetic flux density using finite element method

The MR damper is shaped to guide the magnetic flux axially through the bobbin, across the bobbin flange (active pole) length and gap at one end, through the flux return, and across the gap and bobbin flange again at the opposite end. The fluid volume through which the magnetic field passes is defined as the active volume. The MR effects only occur within the active volume. For most effective dampers, it is needed to have a high magnetic flux density passing through a large active volume.

Table 3
Lower and upper boundaries of the parameters.

Parameter	LB	UB
Flange length (t)	2 mm	7 mm
Gap width (g)	0.4 mm	1.2 mm
Piston head housing thickness (g_h)	1.5 mm	2.5 mm
Radius of piston core (R_c)	6 mm	8 mm
Gap length (L)	18 mm	22 mm
Number of coil turns (N_c)	100 mm	581 mm
Current (I)	0 A	2 A
Radius of piston head (R)	14.5 mm	

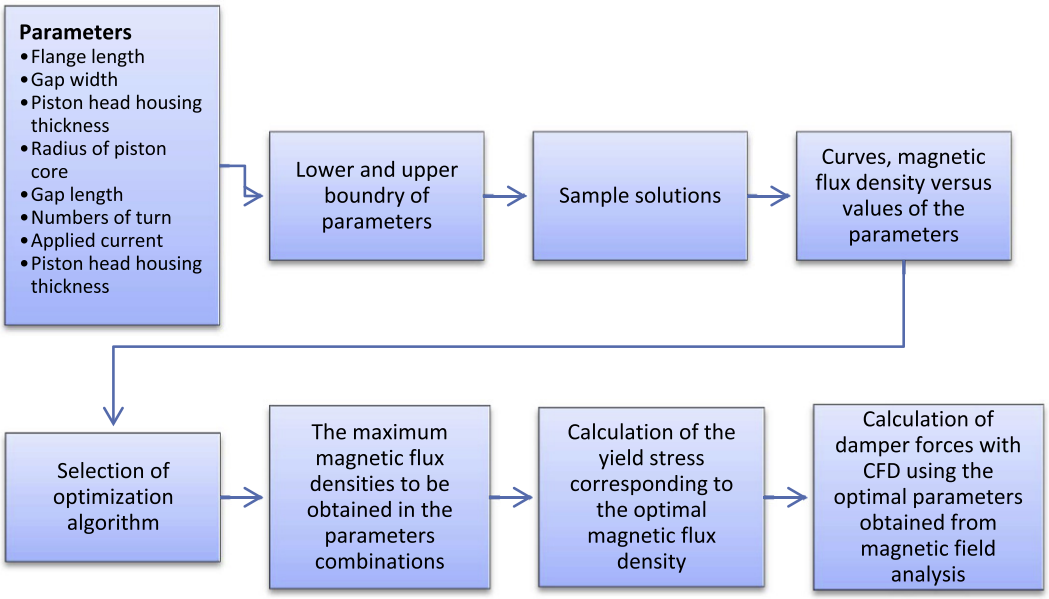

Fig. 16. Optimization study for magnetic field analysis.

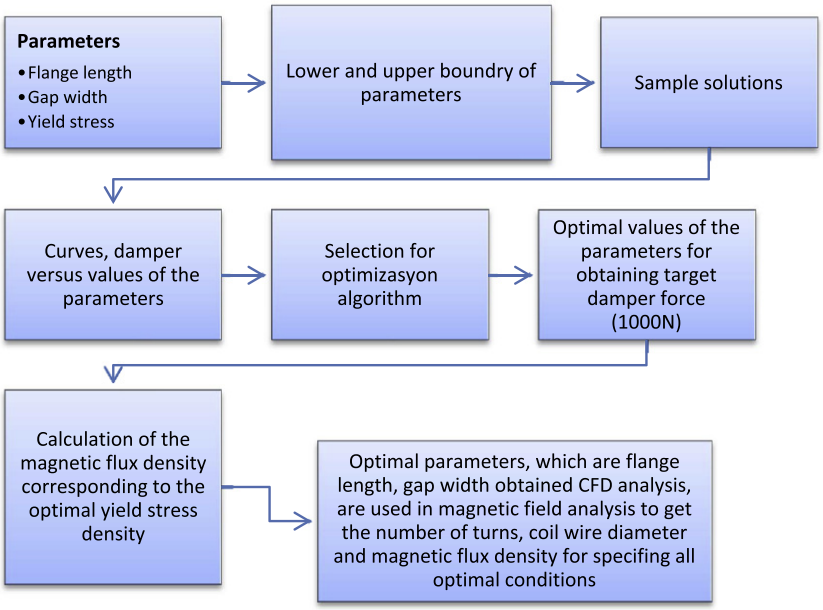

Fig. 17. Optimization study for CFD analysis.

Magnetic flux density in dampers was calculated by FEM analysis that realized by Magnetostatic tool in ANSYS v12.1. A 45° slice of this computational domain was modelled for computational time reduction, and assuming the magnetic flux to be axi-symmetric.

The steps to calculate of magnetic flux density can be seen in Fig. 5.

Geometrical parameters of the piston head can be seen Fig. 6. Where g is gap width, t is flange (pole) length, g_h is piston head housing thickness, W is coil width, L is gap length, R is radius of piston head, R_c is radius of piston core, e is epoxy thickness.

According to varying damper dimensions, computational domain consists of about 90,000 nodes and 64,000 tetrahedral volume elements to solve magnetic analysis (see Fig. 7).

4.1. Results of magnetic field analysis

A damper configuration specified for initial analysis was performed and obtained magnetic flux density (B) at a point in the gap and B was converted to yield stress (τ_y) by Eq. (6) as can be seen in Table 2. Visualized results of the magnetic analysis can be seen in Fig. 8. Intensity of the magnetic flux density in the core

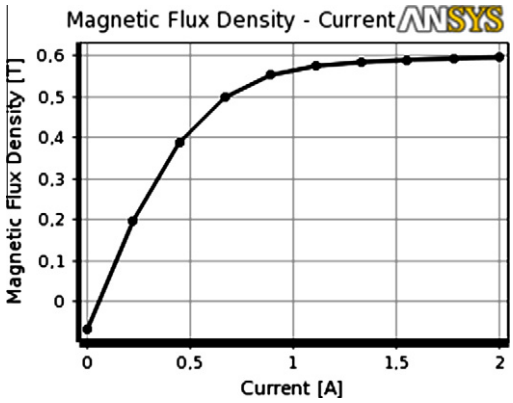

Fig. 18. Magnetic flux density vs. applied current.

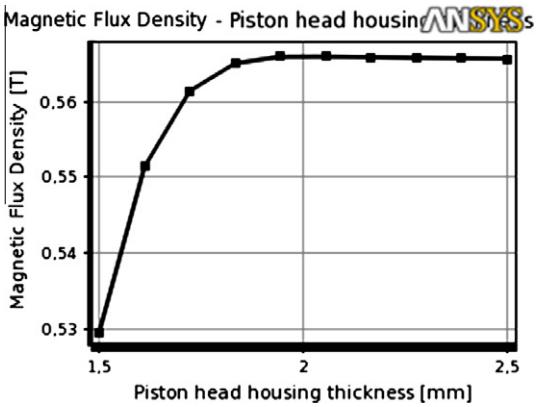

Fig. 21. Magnetic flux density vs. piston head housing thickness.

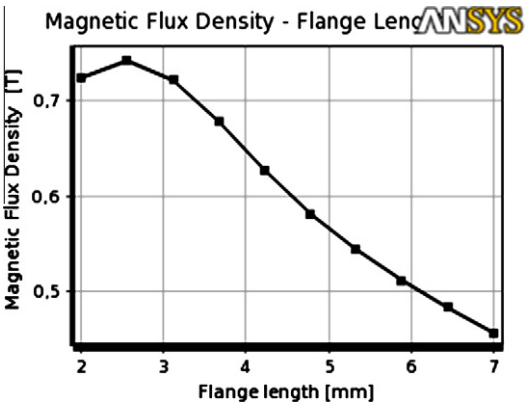

Fig. 19. Magnetic flux density vs. flange length.

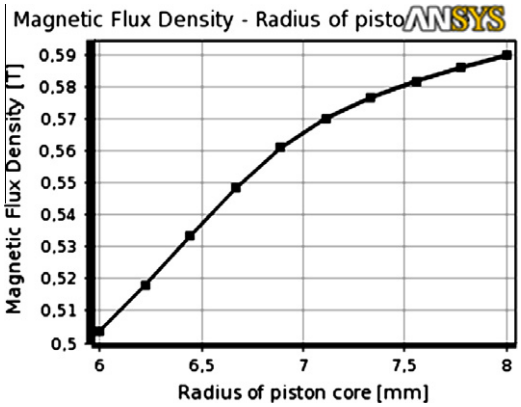

Fig. 22. Magnetic flux density vs. radius of piston core.

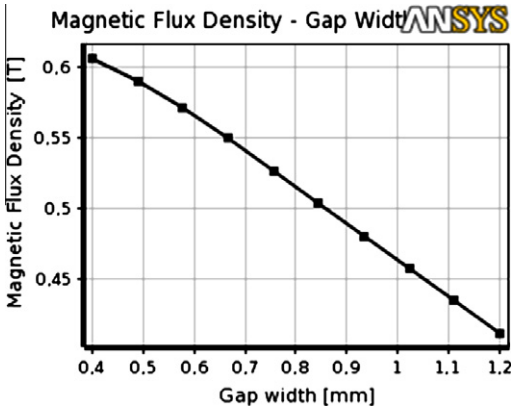

Fig. 20. Magnetic flux density vs. gap width.

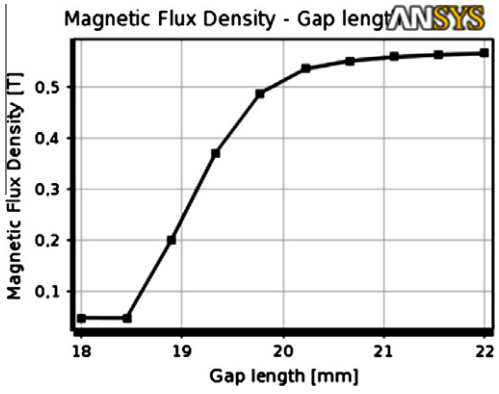

Fig. 23. Magnetic flux density vs. gap length.

of the piston head can be seen in Fig. 8a, while closing to edge the intensity decreases due to turn the effect of the magnetic circuit. Magnetic flux density of MR fluid in the annular gap under magnetic field can be seen in Fig. 8a and b.

5. Finite element analysis of fluid dynamic of MR damper

CFD analysis was carried out CFX tool of ANSYS v.12.1. For computational time reduction, and assuming the fluid flow to be axisymmetric, a 45° slice of the computational domain was modelled. CFD analysis was realized by moving (deformed) mesh and transient methods. Movement of the piston in the cylinder could be simulated due to the moving mesh. The damper force–velocity and damper force–displacement curves were obtained by the transient method so that to compare with experimental data. Regions not under magnetic field (Newtonian) within the gap in parallel to coil and the regions under magnetic field (non-Newtoinan) within the gap in parallel to flange could be defined by CCL's – CFX Command Language – expressions depending on time in the same computational domain. While moving the piston in the domain, it can be specified with the CCL expressions whether a node is in the active region or not.

The steps to realize of CFD analysis can be seen in Fig. 9.

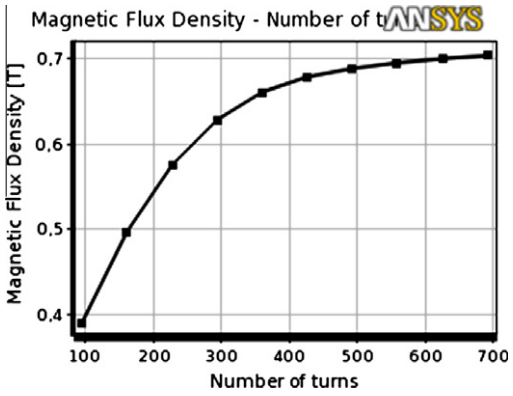

Fig. 24. Magnetic flux density vs. number of coil turns.

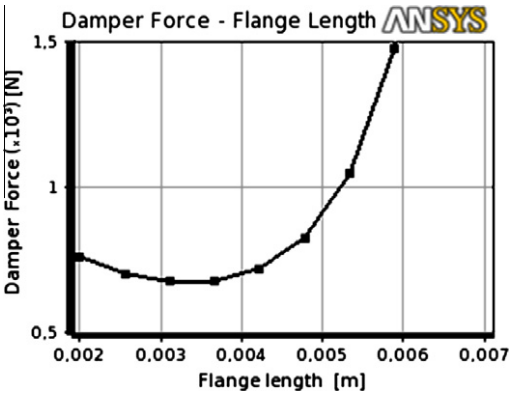

Fig. 27. Damper force vs. flange length.

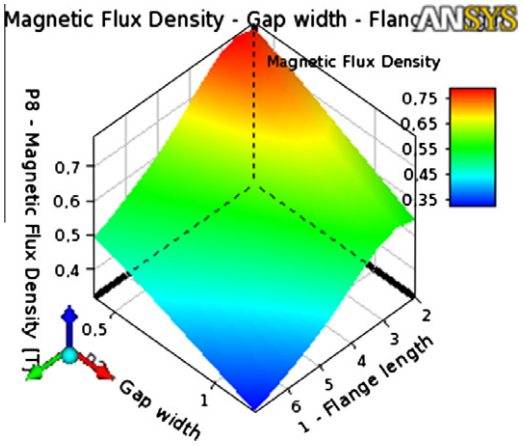

Fig. 25. Surface from magnetic flux density, gap width and flange length.

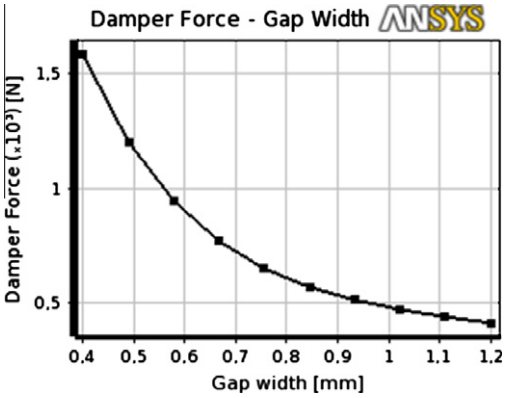

Fig. 28. Damper force vs. gap width.

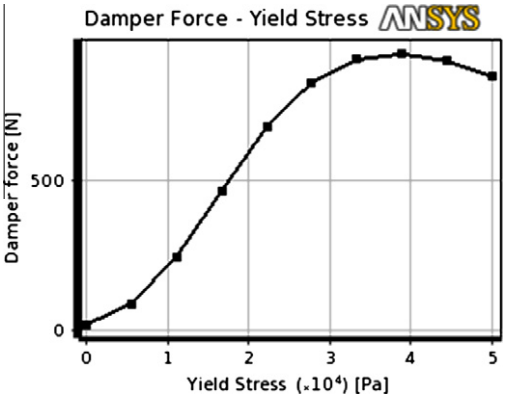

Fig. 26. Damper force vs. yield stress.

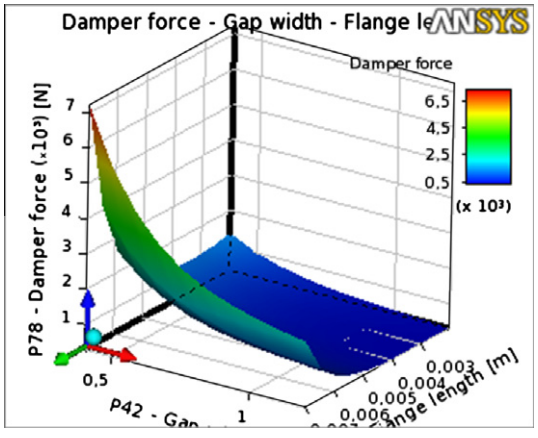

Fig. 29. Surface by damper force, gap width and flange length.

Table 4
Optimal parameters for maximum B.

	t (mm)	g (mm)	g_h (mm)	R_c (mm)	L (mm)	N_c	d_k (mm)	I (A)	B (T)
Candidate damper 1	2.34	0.52	2.22	7.90	21.60	498	0.3	0.5	0.827
Candidate damper 2	2.21	0.55	2.08	7.96	20.97	432	0.32	0.56	0.818
Candidate damper 3	3.04	0.44	2.14	7.71	21.91	292	0.4	0.4	0.594

d_k: Maximum coil wire diameter for the number of coil turns.

According to varying damper dimensions, a computational domain consists of about 6200 nodes and 25,000 tetrahedral volume elements. The mesh and the boundaries can be seen in Fig. 10. Moving parts of the damper, piston and sliding piston, were taken into account while creating the mesh.

Non-Newtonian regions in the gap were described by setting viscosity as material properties on CFX-Pre. The Bingham viscosity is expressed as a variable in the CFD analysis using Bingham CFD model [30] based on Bingham plastic model (see Eq. (1)).

$$\mu_B = \frac{\tau_{y,k}}{\dot{\gamma}} + \mu_p \quad \text{for} \quad \dot{\gamma} \geq \dot{\gamma}_k$$
$$\mu_B = \mu_s \quad \text{for} \quad \dot{\gamma} < \dot{\gamma}_k \tag{8}$$

In Eq. (8) and Fig. 11, $\tau_{y,k}$ is yield stress defines the transition to non-Newtonian region. μ_s is high (solid-type) viscosity, $\dot{\gamma}_k$ is a critical shear rate and is starting point of transition to non-Newtonian from Newtonian.

In pre-yield region viscosity is solid-type viscosity (μ_s) in the Bingham CFD model. After the critical shear rate or critical yield stress is exceeded viscosity decreases to value of the plastic viscosity (Fig. 11). μ_B approaches infinity at low shear rates. $\mu_s > 100 - 1000$ times the plastic viscosity μ_p then a high degree of computational precision is achieved [30]. In the study, it was defined as $\mu_s = 100 \times \mu_p$ in our CFD model.

The angular velocity and frequency are as follows.

$$\omega = \frac{u_{max}}{S_{max}} \tag{9}$$

$$f = \frac{\omega}{2\pi} \tag{10}$$

The total time for a cycle of the piston can be calculated as follows.

$$t_{total} = \frac{1}{f} \tag{11}$$

Sinusoidal movement and velocity of the piston are calculated with the equations following:

$$S = S_{max} - S_{max} \cdot cos(\omega t_s) \tag{12}$$

$$u_p = u_{max} \cdot sin(\omega t_s) \tag{13}$$

where t_s is time step and analyses have been realized using the time step until reaching t_{total}. In the study, time step, stroke and velocity were taken as 0.01 s, 0.0125 m, and 0.05 m/s, respectively.

5.1. Results of the CFD analysis

Some CFD results can be seen in Figs. 12–15. In Fig. 12, variation of pressure in the MR damper at 0.36 s while the piston is moving in the direction of compression can be seen, pressure drop has occurred notably in the annular gap. The dynamic viscosity throughout the active length exposed magnetic field has reached to approximately 1000 Pa s (see Fig. 13). Minimal variation of temperature due to viscous effect that is considered as a heating effect in the CFD analysis can be seen Fig. 14. Velocity of the inactive region in the annular gap is higher than those of active region as can be seen on velocity streamlines in Fig. 15.

Table 5
Damper forces from CFD analysis.

	B (T)	τ_y (Pa)	F (N)
Candidate damper 1	0.827	45,019	894
Candidate damper 2	0.818	44,708	830
Candidate damper 3	0.594	33,913	1080

Table 6
Optimal geometry 1.

t (mm)	g (mm)	g_h (mm)	R_c (mm)	L (mm)	N_c	d_k (mm)	I (A)	B (T)	τ_y (Pa)	F (N)
3	0.44	2.1	7.7	21.9	292	0.4	0.4	0.594	33,913	1080

Table 7
Lower and upper boundaries of the parameters.

Parameter	LB	UB
Flange length (t)	2 mm	7 mm
Gap width (g)	0.4 mm	1.2 mm
Yield stress (τ_y)	0 Pa	50,000 Pa

Table 8
Optimal parameter for 1000 N damper force.

	g (mm)	t (mm)	τ_y (Pa)	F (N)
Objective	No	No	Minimum	1000 N
Candidate damper 4	0.52	6	28,208	1045.7

Table 9
Magnetic flux density, number of coil turns and current.

	τ_y (Pa)	B (T)	N_c	d_k (mm)	I (A)
Candidate damper 4	28,208	0.504	175	0.45	1.6

Table 10
Optimal geometry 2.

t (mm)	g (mm)	N_c	d_k (mm)	I (A)	B (T)	τ_y (Pa)	F (N)
6	0.52	187	0.45	1.6	0.504	20,208	1045.7

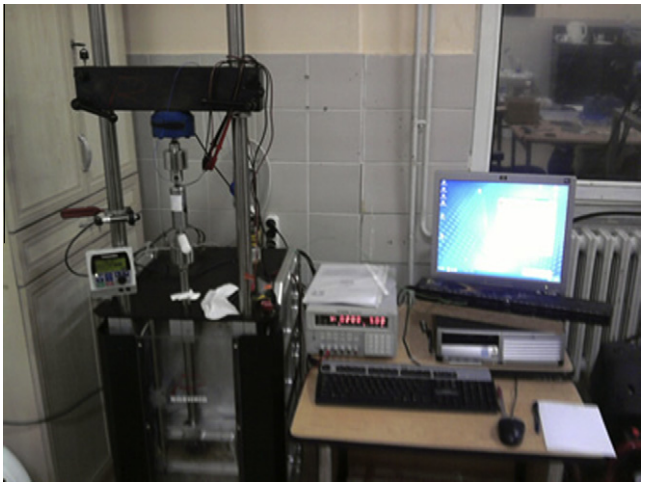

Fig. 30. The test machine with the damper under test.

Fig. 31. Manufactured optimal dampers.

6. Optimization with FEM of magnetic field and fluid dynamic

Optimization method that would be carried out by experimental data has accompanied manufacture difficulty and high cost. A large number of parameters that would be specified to find optimal geometry require the manufacturing of many dampers and then it becomes more costly. Because of the constraints, optimum geometry has been searched by numerical methods in the study. The optimization strategy can be seen schematically in Figs. 16 and 17 for electromagnetic and CFD, respectively.

6.1. Optimization study with magnetic field analysis

In the analysis, the values of parameters that would be yielded maximum magnetic flux density are evaluated as optimal damper geometry. Multi objective genetic algorithm (MOGA) was used in ANSYS Goal Driven Optimization tool as optimization algorithm. The design parameters were searched between lower and upper boundaries as can be seen Table 3.

Seventy-nine sample solutions were realized by ANSYS then the curves of magnetic flux density vs. one of the parameters while keeping constant other parameters could be plotted between the lower and upper boundaries (Figs. 18–29). The magnetic flux density, which changes with the applied current exponentially, especially increases linearly up to 1 A, however, this rising decays gradually between 1 A and 2 A due to saturation (Fig. 18). The flange length through which flux lines pass to perpendicular to the flow direction that causes a field-dependent resistance on the MR flow is critical size. Because it is necessary to keep the magnetic flux density constant throughout the circuit, any magnitude of the magnetic field has to also pass in smaller flange length that cause bigger magnetic flux density on the MR fluid in the gap (Fig. 19). The magnetic flux density is inversely proportional to the gap width in Fig. 20 and it can be seen parallel in the Eq. (7). The magnetic flux density remains insensitive as from 2 mm of piston head housing thickness (Fig. 21). The magnetic flux density changes almost linearly with radius of piston core, however the total value of the increasing is about 0.04 T, which corresponds to increasing of 2 mm of the radius of the piston core (Fig. 22). As can be seen in Fig. 23 the gap length has a significant effect on the magnetic flux density, increasing of approximately 3 mm of the gap length gets increasing of approximately 0.6 T of magnetic flux density. The number of coil turns has an exponential effect on magnetic flux density can be seen Fig. 24.

6.1.1. Optimal parameters obtained by magnetic field analysis

Optimal design parameters, which provide targeted maximum magnetic flux density, suggested by ANSYS as three candidate dampers can be seen in Table 4.

The magnetic flux density of the candidate dampers was converted to yield stress using Eq. (6) and the values of the yield stress together with values of gap width and flange length in Table 4 have

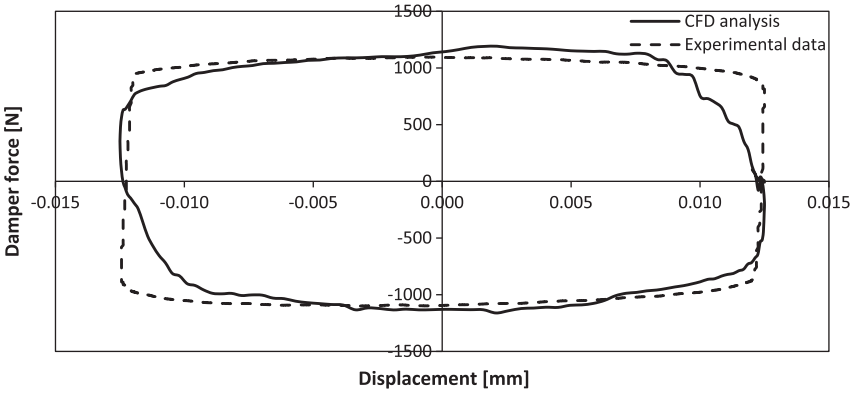

Fig. 32. Damper force vs. displacement by comparison with experimental data and CFD analysis for optimal damper 1.

been employed to CFD to obtain damper force under the optimal conditions (Table 5).

It can be seen in examining of the candidate damper that the candidate damper 1 and 2 cannot be close to the desired damper force, 1000 N. Besides providing desired damper force the candidate damper 3 that can be realized with less the applied current and the magnetic flux density than the others is specified optimal damper in the optimization study of magnetic field analysis (see Table 6).

6.2. Optimization study with CFD analysis

In the analysis, the values of parameters that would be yielded targeted damper force, 1000 N, are evaluated as optimal damper geometry. Multi objective genetic algorithm (MOGA) was used in ANSYS Goal Driven Optimization tool as optimization algorithm. The design parameters were searched between lower and upper boundaries as can be seen Table 7.

Fifteen sample solutions were realized by ANSYS and then curves of damper force vs. one of the parameters while keeping constant other parameters between the lower and upper boundaries (Figs. 26–28). In Fig. 26 can be seen that while increasing the yield stress damper force increases linearly up to 30,000 Pa of the yield stress, however, this rising decays gradually at higher the applied current between 30,000 Pa and 40,000 Pa, after the value damper force decreases due to saturation. In little values of flange length give lower damper force expectedly from Eq. (4), it implies that controllable force increases with flange length (Fig. 27). According to Eq. (3) increasing of gap width decreases damper force as validation in Fig. 28 from CFD analysis. However, increasing of the damper force is related to uncontrollable force, this is not desirable.

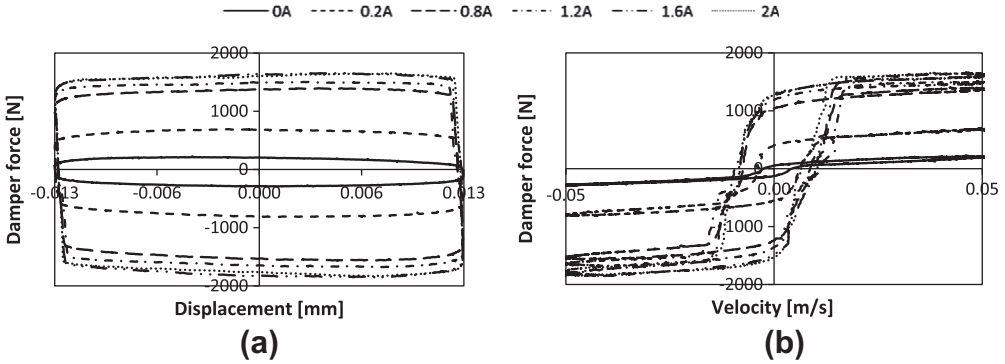

Fig. 33. Curves of (a) Damper force vs. displacement and (b) Damper force vs. velocity of optimal damper 1 for currents of 0 A, 0.2 A, 0.8 A, 1.2 A, 1.6 A, 2.0 A.

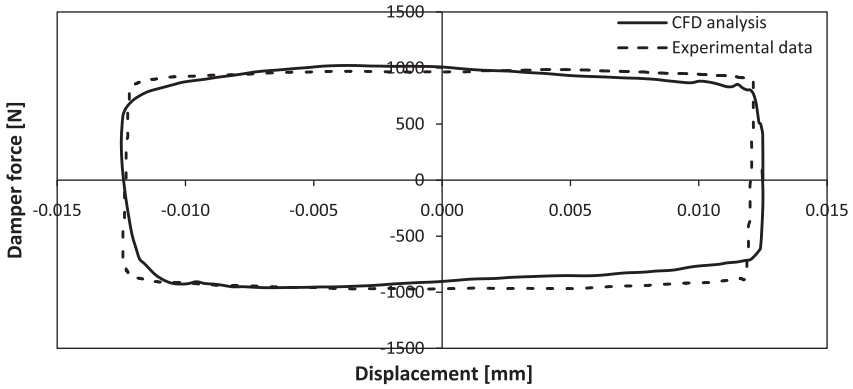

Fig. 34. Damper force vs. displacement by comparison with experimental data and CFD analysis for optimal damper 2.

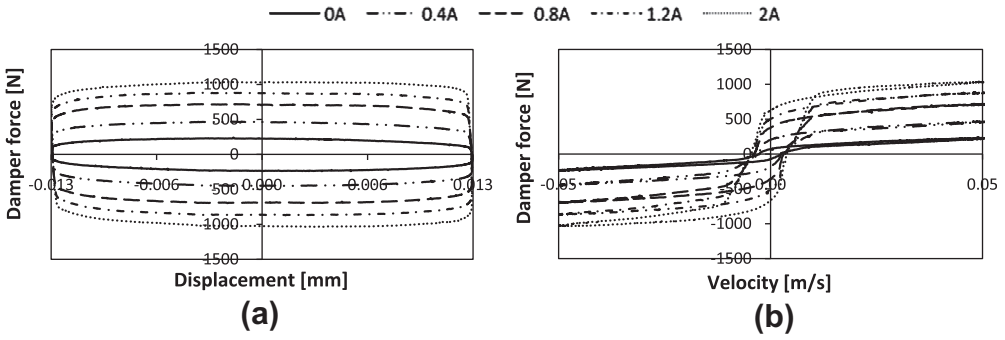

Fig. 35. Curves of (a) damper force vs. displacement and (b) damper force vs. velocity of optimal damper 2 for currents of 0 A , 0.4 A, 0.8 A, 1.2 A, 2.0 A.

6.2.1. Optimal parameters obtained by CFD analysis

Optimal design parameters, which provide targeted damper force, suggested by ANSYS can be seen in Table 8.

Yield stress of the candidate damper is converted to magnetic flux density using Eq. (6). The yield stress and current and the number of coil turns calculated by keeping constant g_h (2 mm), R_c (7 mm), L (22 mm) and d_k (0.45 mm) can be seen in Table 9.

Candidate damper 4 was selected as optimal geometry (see Table 10).

7. Confirmation of the optimization studies

Two optimal dampers specified the FEM analyses were manufactured and tested to validate the values of damper forces (see Fig. 31). The dampers were tested on shock machine Roehrig MK-2150. The shock machine has its own software (SHOCK 6.3) to collect data which curves are force vs. time, force vs. velocity, and force vs. displacement. A programmable power supply (GWinstek PPE 3223) was used to feed current to coil of the MR dampers (see Fig. 30).

The test results are compared with the results of CFD analysis in Figs. 32 and 34 for optimal geometry 1, and optimal geometry 2, respectively. A good agreement has been observed between the experimental and simulated data.

In addition to, curves of damper force vs. displacement and damper force vs. velocity at some values of current for the Optimal damper 1 and Optimal damper 2 can be seen in Figs. 33 and 35, respectively. As can seen in Fig. 33, damper force at 1.6 A is slightly greater than the one at 2 A for optimal damper 1 due to saturation and high temperature that arises at high current values and affects damper performance negatively.

8. Conclusion

The purpose of the study was to optimize MR damper geometrically in accordance with two objectives, target damper force as 1000 N and maximum magnetic flux density. The optimization studies were carried out by finite element method using electromagnetic and CFD tools of ANSYS v12.1. The FEM analyses were employed to get desired optimal values in ANSYS Goal Driven Optimization tool. Values of optimal of the design parameters of the MR damper were searched between lower and upper boundaries in both electromagnetic and CFD analyses. The parameters were geometrical magnitudes, current excitation and yield stress.

In the electromagnetic analysis gap width, flange length, gap length, piston head housing thickness, radius of piston core, the number of coil turns and the applied current were selected as design parameters to be able to get maximum magnetic flux density. The values were used in CFD analysis to obtain damper force under optimal conditions. Optimal damper was specified as $g = 0.44$ mm, $t = 3$ mm, $I = 0.4$ A and under these conditions damper force became 1080 N.

In the CFD analysis gap width, flange length and yield stress were selected as design parameters to be able to get targeted damper force with their optimal values. The values were used in electromagnetic analysis to obtain magnetic flux density, the number of coil turns and the applied current. Optimal damper was determined as $g = 0.52$ mm, $t = 6$ mm, $I = 1.6$ A and under these conditions damper force became 1045.7 N.

The analysis method can be described briefly as follows; Optimal parameters obtained electromagnetic analysis were employed in CFD analysis thus damper force could be calculated. Similarly, optimal parameters obtained CFD were employed in electromagnetic analysis thus magnetic flux density, the number of coil turns and the applied current could be calculated.

Thanks to the CFD analysis performed with deformed (moving) mesh and transient method, rebound and compression movement of piston could be modelled as in real work of the damper. In addition to, flow magnitudes (flow velocity, pressure, dynamic viscosity, temperature shear rate, etc.) at any position of the piston could be obtained easily. In the CFD analysis, Bingham plastic model was employed to model flow of non-Newtonian region. Value of yield stress in Bingham plastic model varies with the applied current was obtained by magnetic flux density, which is converted to yield stress. Also, to be able to catch up non-Newtonian regions in the piston head for any time in moving mesh, CCL expressions were written in ANSYS CFX.

Optimal damper configurations obtained at the end of FEM analyses were manufactured and then tested. Test results showed that the optimal dampers have provided to the expected damper force and that a good agreement has been observed between the experimental and simulated data.

A new method was presented to get the optimal design of MR damper with the finite element analyses. The method that uses both electromagnetic and CFD can be determined optimal design parameters of a MR damper getting damper force desired and maximum magnetic field that provides maximum controllability of the MR damper.

Acknowledgements

The authors gratefully acknowledge TUBITAK for making this project possible under Grant No: 104M157 and Sakarya University for BAPK Project No: 2007-50-02-003.

References

[1] Wereley NM, Pang L. Non-dimensional analysis of semi-active electrorheological and magnetorheological dampers using approximate parallel plate models. Smart Mater Struct 1998;5(7):732–43.
[2] Felt DW, Hagenbuchle M, Liu J, Richard J. Rheology of a magnetorheological fluid. J Intell Mater Syst Struct 1996;5(7):589–93.
[3] Dimock GA, Lindler JE, Wereley NM. Bingham biplastic analysis of shear thinning and thickening in magnetorheological dampers. Smart Struct Mater 2000;3985:444–55.
[4] Hesselbach H, Abel-Keilhack C. Finite element flow analysis of magnetic fluids with yield stress, Book of Abstracts des 5. Deutschen Ferrofluid-Workshop, Mühlheim/Ruhr; 2003. p. 15–6.
[5] Wang X. Nonlinear behavior of magnetorheological (MR) fluids and MR dampers for vibration control of structural systems. PhD thesis. Reno: University of Nevada; 2002.
[6] Wang X, Gordaninejad F. Flow analysis and modeling of field-controllable electro- and magneto-rheological fluids dampers. J Appl Mech 2007;74(1):13–22.
[7] Yasrebi N, Ghazavi A, Mashhadi MM. Magneto-rhelogical fluid dampers modeling: numerical and experimental. In: Proceeding of the 17th IASTED international conference modeling and, simulation; May 24–26, 2006.
[8] Widjaja J, Samali B, Li J. Electrorheological and magnetorheological duct flow in shear-flow mode using Herschel–Bulkley constitutive model. J Eng Mech 2003;129(12):1459–65.
[9] Ericksen EO, Gordaninejad F. A magneto-rheological fluid shock absorber for an off-road motorcycle. Int J Vehicle Des 2003;33:138–52.
[10] Li WH, Du H. Design and experimental evaluation of a magnetorheological brake. Int J Manuf Technol 2003;21:508–15.
[11] Ellam DJ, Atkin RJ, Bullough WA. Analysis of a smart clutch with cooling flow using two-dimensional Bingham plastic analysis and computational fluid dynamics. Proc IMechE, Power Energy 2005;219(8):639–52.
[12] Susan-Resiga D. A rheological model for magneto-rheological fluids. J Intell Mater Syst Struct 2009;20(8):1001–10.
[13] Hitchcock GH, A novel magneto-rheological fluid damper. Master thesis. Mechanical Engineering Department. Reno: University of Nevada; 2002.
[14] Zhang HH, Liao CR, Chen WM, Huang SL. A magnetic design method of MR fluid dampers and FEM analysis on magnetic saturation. J Intell Mater Syst Struct 2006;17(8–9):813–8.
[15] Nguyen QH, Han YM, Choi SB, Wereley NM. Geometry optimization of MR valves constrained in a specific volume using the finite element method. Smart Mater Struct 2007;16(6):2242–52.

[16] Nguyen QH, Choi SB, Wereley NM. Optimal design of magnetorheological valves via a finite element method considering control energy and a time constant. Smart Mater Struct 2008;17(2):025024 [12pp].
[17] Nguyen QH, Choi SB. Optimal design of a vehicle magnetorheological damper considering the damping force and dynamic range. Smart Mater Struct 2009;18(1):015013.
[18] Nguyen QH, Choi SB. Dynamic modeling of an electrorheological damper considering the unsteady behavior of electrorheological fluid flow. Smart Mater Struct 2009;18(5):055016 [8pp].
[19] Yang L, Duan F, Eriksson A. Analysis of the optimal design strategy of a magneto-rheological smart structure. Smart Mater Struct 2008;17(1):015047 [8pp].
[20] Karakoc K, Park EJ, Suleyman A. Design considerations for an automotive magnetorheological brake. Mechatronics 2008;18:434–47.
[21] Grundwald A, Olabi AG. Design of magneto-rheological valve. Sensors Actuator 2008;148:211–23.
[22] Parlak Z, Engin T, Şahin İ, Çallı İ. Geometric optimisation of vehicle shock dampers with magnetorheological fluid. Int J Vehicle Des 2010;54(4):371–92.
[23] Lord Corporation. MRF-132DG Magneto-rheological fluid; 2008. <http://www.lordfulfillment.com/upload/DS7015.pdf>.
[24] Çeşmeci Ş, Engin T. Modeling and testing of a field-controllable magnetorheological fluid damper. Int J Mech Sci 2010;52(8):1036–46.
[25] Rosenfeld NC, Wereley NM. Volume-constrained optimization of magnetorheological and electrorheological valves and dampers. Smart Mater Struct 2004;13:1303–13.
[26] Delivorias. RP 2004 Application of ER and MR fluid in an automotive crash energy absorber Eindhoven University of Technology, Department of Mechanical Engineering (Eindhoven), Report No MT0418.
[27] Lord Corporation. MR Fluid Product Bulletins; 2008. <http://www.rheonetic.com/fluidbegin.htm>.
[28] Nguyen QN, Choi SB. Optimal design of MR shock absorber and application to vehicle suspension. Smart Mater Struct 2009;18(3):035012.
[29] Salvetti M. Detector solenoid: thermal and structural analyses magnet documents; 2004. <http://meco.ps.uci.edu/old/magnet_docs/mm056.pdf>.
[30] Bullough WA, Elam DJ, Wong AP, Tozer RC. Computational fluid dynamics in the flow of ERF/MRF in control devices and of oil through piezo-hydraulic valves. Comput Struct 2008;86(3–5):266–80.